Nucleation and cavitation of spherical, cylindrical, and slablike droplets and bubbles in small systems

Luis G. MacDowell[a)]
Departamento de Química Física, Facultad de Ciencias Químicas, Universidad Complutense, 28040 Madrid, Spain

Vincent K. Shen
Physical and Chemical Properties Division, National Institute of Standards and Technology, MS 8380 Gaithersburg, Maryland 20899-8380

Jeffrey R. Errington
Department of Chemical and Biological Engineering, University at Buffalo, The State University of New York at Buffalo, New York 14260-4200

Computer simulations are employed to obtain subcritical isotherms of small finite sized systems inside the coexistence region. For all temperatures considered, ranging from the triple point up to the critical point, the isotherms gradually developed a sequence of sharp discontinuities as the system size increased from ~8 to ~21 molecular diameters. For the smallest system sizes, and more so close to the critical point, the isotherms appeared smooth, resembling the continuous van der Waals loop obtained from extrapolation of an analytic equation of state outside the coexistence region. As the system size was increased, isotherms in the chemical potential-density plane developed first two, then four, and finally six discontinuities. Visual inspection of selected snapshots revealed that the observed discontinuities are related to structural transitions between droplets (on the vapor side) and bubbles (on the liquid side) of spherical, cylindrical, and tetragonal shapes. A capillary drop model was developed to qualitatively rationalize these observations. Analytic results were obtained and found to be in full agreement with the computer simulation results. The analysis shows that the shape of the subcritical isotherms is dictated by a single characteristic volume (or length scale), which depends on the surface tension, compressibility, and coexistence densities. For small reduced system volumes, the model predicts that a homogeneous fluid is stable across the whole coexistence region, thus explaining the continuous van der Waals isotherms observed in the simulations. When the liquid and vapor free energies are described by means of an accurate mean-field equation of state and surface tensions from simulation are employed, the capillary model is found to describe the simulated isotherms accurately, especially for large systems (i.e., larger than about 15 molecular diameters) at low temperature (lower than about 0.85 times the critical temperature). This implies that the Laplace pressure differences can be predicted for drops as small as five molecular diameters, and as few as about 500 molecules. The theoretical study also shows that the extrema or apparent spinodal points of the finite size loops are more closely related to (finite system size) bubble and dew points than to classical spinodals. Our results are of relevance to phase transitions in nanopores and show that first order corrections to nucleation energies in finite closed systems are power laws of the inverse volume. © *2006 American Institute of Physics*. [DOI: 10.1063/1.2218845]

I. INTRODUCTION

Since the advent of computer simulations,[1] the influence of finite size effects has been a major concern.[2] In the study of phase transitions,[3,4] peculiar rounding effects in the freezing of hard spheres were noted a long time ago. Alder and Wainwright found that the liquid and solid branches of the equation of state were connected by a continuous loop, reminiscent of the mean-field van der Waals loop.[5] The meaning of this loop and its essentially system-size-dependent nature was explained later by Mayer and Wood.[6] These authors noted that a discontinuity of the pressure and the appearance of a portion of the isotherm with negative susceptibility were the signatures of droplet formation in small systems (see Ref. 7 for a more elaborate account of these results).

The question concerning the conditions under which a droplet is stable became of great interest some time after, particularly in computer simulation studies of nucleation,[8–10] a topic which has lately attracted much interest.[11–16] While the appearance of a loop in the chemical potential-density plane may be considered a finite size artifact, from a practical point of view, it allows for the calculation of droplet free energies by thermodynamic integration.[17] Furthermore, with ever-increasing interest in nanotechnology, and the improved control in the design of porous materials,[18] the phase behav-

---
[a)]Electronic mail: luis@ender.quim.ucm.es

ior and equation of state of small systems has become a topic of great interest, allowing, for example, characterization of pore dimensions.[19]

For these reasons, the study of droplet stabilization and the related loops in the equation of state has received renewed interest in recent years.[20–28] Great effort has been devoted to study this problem using the Ising model,[20,21,24] where the discrete nature of the magnetization makes it possible to study extremely large systems,[24] and the symmetry properties of its Hamiltonian allow for some simplifications in the theoretical analysis.[23] For continuum models, efforts have concentrated mainly on the Lennard-Jones fluid,[25–28] but the simulations are considerably more time consuming. Therefore, a large amount of data remains lacking which prevents the testing of theoretical treatments over a wide range of conditions.

In this work, we employ a very powerful sampling technique, transition-matrix Monte Carlo, to compute finite size isotherms of the Lennard-Jones fluid over a broad range of system sizes and temperatures. The simulation results are rationalized using analytic theoretical results based on the capillary drop model.[29] To this end, we extend previous analysis of the droplet condensation transition,[25,26,28] in order to account for bubble formation. Furthermore, we present a generalized treatment, which accounts for the formation of "droplets" and "bubbles" of different shapes (spheres, cylinders, and slabs). The theoretical results allow us to explain the series of discontinuities observed in the finite size isotherms generated by simulation and to obtain finite size corrections to nucleation energies measured in closed systems of finite size.

The paper is organized as follows. Section II is devoted to the theoretical description of subcritical isotherms, with Table I summarizing main findings. Section III presents the model employed and briefly discusses the simulation methodology. The simulation results and a comparison with theory are presented in Sec. IV, while a summary with the main conclusions of this work is given in Sec. V. An appendix is devoted to present algebraic manipulations employed to obtain the analytical results of Sec. II.

II. THEORETICAL ANALYSIS

A. General solution

1. Preliminary definitions

Without loss of generality, let us study the formation of a bubble from a stretched liquid. The analogous case of the formation of a droplet from a supersaturated vapor is simply recovered by interchanging the labels l and v. We consider a fluid inside a closed system of volume V, containing overall N particles. We allow the system to adopt either of two possible states. The first one is a homogeneous state of uniform density ρ and Helmholtz free energy A_{hom}. The second one is an inhomogeneous or bubble state, with Helmholtz free energy A_{inh}, consisting of liquid and vapor domains of volume, V_l and V_v, respectively. Within a capillary drop approximation we expect that both domains attain densities $\rho_l = \rho_l(\mu)$ and $\rho_v = \rho_v(\mu)$ which correspond to their bulk values at the specified chemical potential μ. Henceforth, we restrict our

discussion to the case were the surface area of the cavitated domain, S_{lv}, is given in terms of the bubble volume as $S_{lv} = k_g V_v^n$, where k_g is a geometrical constant and n is a rational number. With this restriction, we can write the Helmholtz free energy difference between the inhomogeneous and homogeneous states as[26,29–32]

$$\Delta A = [(\mu(\rho_v) - \mu(\rho))\rho - (p(\rho_v) - p(\rho))]V$$
$$- [p(\rho_l) - p(\rho_v)]V_l + k_g \gamma V_l^n, \tag{1}$$

where γ is the surface tension. Note that the above equation neglects capillary wave fluctuations, which are known to have some effect.[24]

2. Solution of the Laplace equation

The derivative of the Helmholtz free energy for the inhomogeneous state with respect to changes in the bubble volume is given by[33]

$$\left(\frac{\partial A_{\mathrm{inh}}}{\partial V_v}\right)_{NVT} = \Delta p - n k_g \gamma V_v^{n-1}, \tag{2}$$

where Δp is the Laplace pressure difference, $p_v - p_l$; $p_v = p(\rho_v)$ and $p_l = p(\rho_l)$ are the vapor and liquid pressures, respectively, and we have considered a negligible adsorption at the surface of tension.[26,32]

In the case of a closed system, solving for the roots of the above equation is not trivial because one cannot change V_v without changing the chemical potential, and hence, Δp. In general, the vapor and liquid densities may depart from their coexistence values, ρ_v^c and ρ_l^c, by an amount which depends on the actual chemical potential. To first order, we may write

$$\rho_l = \rho_l^c + \chi_l \Delta \mu, \tag{3}$$

where χ_l, the chemical potential derivative of ρ at ρ_l^c, is related to the isothermal compressibility κ as $\chi = \rho^2 \kappa$, while $\Delta \mu = \mu - \mu_c$. Therefore, the bubble volume fraction $t = V_v / V$ may be expressed as

$$t = \frac{\Delta \rho - \chi_l \Delta \mu}{\Delta \rho_c}, \tag{4}$$

where $\Delta \rho = \rho - \rho_l^c$, $\Delta \rho_c = \rho_v^c - \rho_l^c$, and we have assumed that $\chi_l - \chi_v$ is negligible. The latter assumption is exact for a symmetric fluid, such as the Ising model, and becomes increasingly accurate for an ordinary fluid approaching the critical point.[2]

Substitution of Eq. (4) into Eq. (2), followed by some rearrangement, yields the following result for the Laplace equation:

$$\chi_l \Delta \mu^{2-n/1-n} - \Delta \rho \Delta \mu^{1/1-n} + \left(\frac{n k_g \gamma}{\Delta \rho_c^n V^{1-n}}\right)^{1/1-n} = 0, \tag{5}$$

where use has been made of the Gibbs-Duhem equation in order to relate changes in chemical potential with those in pressure as $\Delta p = \Delta \rho_c \Delta \mu$. We could now solve for $\Delta \mu$ as a function of $\Delta \rho$ and V, as in Ref. 26. However, it is possible to rearrange the equation so that it adopts a universal form:

$$x^{2-n/1-n} - x^{1/1-n} + K_n = 0, \tag{6}$$

where x is a reduced chemical potential and K_n is a reduced system size:

$$x = \frac{\chi_l}{\Delta\rho}\Delta\mu,$$

$$K_n = \left(\frac{nk_g\gamma\chi_l}{\Delta\rho_c^n\Delta\rho^{2-n}V^{1-n}}\right)^{1/1-n}. \tag{7}$$

Although the solutions of Eq. (6) are not generally known, exact asymptotic limits may be found (Appendix). One particularly remarkable conclusion is that the equation cannot be satisfied unless $K_n < (1-n)/(2-n)^{2-n/1-n}$. Physically, this means that at a given density, the system may only separate into two different phases for large enough system volumes. In the next section, we will consider three specific cases, $n=2/3$, $n=1/2$, and $n=0$, which correspond to the formation of a spherical, a cylindrical, and a tetragonal (slab) bubble, respectively. In principle, other geometries, such as ellipsoidal bubbles, could also be envisaged.[24,34] However, this renders the problem much more complicated mathematically, and will not be considered here.

3. Free energy

In order to estimate the free energy of the inhomogeneous states, it will prove necessary to obtain an expression that is consistent with the approximations introduced into the Laplace equation. To achieve this goal, we solve for $\Delta\mu$ using Eq. (4), then substitute into Eq. (2), and integrate, giving the following result for the free energy difference between an inhomogeneous state with a bubble of size V_v and the corresponding homogeneous state ($V_v=0$):

$$\Delta A(V_v) = -\frac{\Delta\rho_c\Delta\rho}{\chi_l}V_v + \frac{1}{2}\frac{\Delta\rho_c^2}{\chi_l}\frac{V_v^2}{V} + k_g\gamma V_v^n. \tag{8}$$

Similar to the Laplace equation, the expression for the free energy may also be rearranged to yield a universal scaled energy:

$$\Delta a(w) = w^2 - w + \frac{2^{n-1}}{n}K_n^{1-n}w^n, \tag{9}$$

where

$$w = \frac{1}{2}\frac{\Delta\rho_c}{\Delta\rho}t$$

$$\Delta a = \frac{1}{2}\frac{\chi_l}{\Delta\rho^2}\frac{\Delta A}{V}. \tag{10}$$

For the particular case of $n=2/3$, the scaled energy adopts the form suggested by Biskup et al. for spherical droplets.[22] Since the equilibrium values of w only depend on the constant K_n, the equilibrium free energy will adopt a universal scaling form dependent only on K_n. The scaling behavior of the droplet free energy has been also discussed by Binder.[23]

B. Spherical bubble

For the formation of an incipient new phase of spherical shape, the geometrical constant relating the surface area to its volume is $k_g^3 = 36\pi$, while $n=2/3$. Therefore, the solutions of the Laplace equation [Eq. (6)] are given by the roots of a quartic polynomial.

1. Solutions of the Laplace equation

For the case of a vapor phase formed from a liquid, solving Eq. (6) together with Eq. (3) shows that a spherical bubble may be partially or absolutely stable ($\Delta A > 0$ or $\Delta A < 0$, respectively), only when the overall density of the system is smaller than a threshold density ρ^* given by (Appendix)

$$\rho^* = \rho_l^c + 4\Delta\rho_c\left(\frac{\xi_{sph}}{V}\right)^{1/4} \quad \text{with} \quad \xi_{sph} = \frac{8}{729}\frac{k_g^3\gamma^3\chi_l^3}{\Delta\rho_c^6}. \tag{11}$$

For consistency with previous work,[26] we have defined a characteristic volume, ξ_{sph}, which governs the deviations of ρ^* away from ρ_l^c. Note that this volume is specific to bubble formation. For the case of droplet formation, the label transformation from $l \to v$ is required. Neglecting ρ_v^c, such that $\Delta\rho_c = \rho_l^c$, and assuming that the vapor is an ideal gas, $\chi_v = \rho_v^c/kT$, we recover the result obtained in Ref. 26.

For densities larger than ρ^*, the Laplace equation has two possible solutions. One corresponds to the formation of an unstable bubble, while the other corresponds to the formation of a partially or eventually absolutely stable bubble. If the limiting behavior of large $|\Delta\rho|$ is sought, the asymptotic behavior of the stable and unstable solutions must be considered separately. For the unstable solution, the exact limiting result is (Appendix)

$$\rho_l - \rho_l^c = (\rho - \rho_l^c)\left\{1 - 27\frac{\xi_{sph}}{V}\left(\frac{\Delta\rho_c}{\Delta\rho}\right)^4\right\}. \tag{12}$$

The result shows that for large ρ, the density of the liquid surrounding the unstable bubble approaches asymptotically the total density of the system, meaning that the cavitation event takes place with negligible density change. This effect is more pronounced for large volumes, so that the NVT ensemble asymptotically approaches the scenario expected in the grand canonical ensemble. For the stable solution, the exact limiting result is (Appendix)

$$\rho_l - \rho_l^c = (\rho - \rho_l^c)\left(\frac{\xi_{sph}}{V}\right)^{1/3}\left(\frac{\Delta\rho_c}{\Delta\rho}\right)^{4/3}. \tag{13}$$

Thus, for either large volume or large ρ, the liquid in equilibrium with a bubble approaches the coexisting liquid density expected in the thermodynamic limit. The significance of this result is perhaps more transparent if we write it in terms of the volume fraction occupied by the bubble. Using Eqs. (3) and (4), we find

$$\frac{V_v}{V} = \frac{\rho - \rho_l^c}{\rho_v^c - \rho_l^c}\left\{1 - \left(\frac{\xi_{sph}}{V}\right)^{1/3}\left(\frac{\Delta\rho_c}{\Delta\rho}\right)^{4/3}\right\}. \tag{14}$$

As expected, for large system sizes the result asymptotically tends to that predicted by the lever rule. The infinite system

behavior, however, is reached at a very slow rate. Most noticeably, the chemical potential of the liquid will remain below μ_c at $\rho = \frac{1}{2}(\rho_l^c + \rho_v^c)$, and will remain so even at lower densities, i.e., well inside the vapor side of the coexistence region. Analogous behavior occurs during the formation of a spherical droplet, so that hysteresis effects can occur if no other mechanism, apart from (spherical) bubble and droplet formations, is available for the system to decay to $\mu = \mu_c$.

2. Free energy

In Sec. II B 1, we have seen that above the threshold density ρ^*, bubble states may become partially or absolutely stable. We will now consider the transition density ρ^t, where the bubble state becomes absolutely stable for the first time. At this density, the system will experience a transition from the homogeneous state to the bubble state in the infinitely long time limit. This transition is analogous to the "catastrophic crystal growth" observed by Swope and Andersen in their study of crystal nucleation.[35] As noted by these authors, the unstable nucleus formed previously is the analog of the nucleation event in an infinite system.

By exploiting the fact that the roots of the scaled free energy [Eq. (9)] obey an equation similar to Eq. (6), we find the exact result for the transition density:

$$\rho^t = \rho^* + ((2)(3^{3/4}) - 4)\Delta\rho_c\left(\frac{\xi_{\text{sph}}}{V}\right)^{1/4}. \tag{15}$$

The scaling behavior of Eq. (15) has been recently confirmed for the Lennard-Jones fluid.[26,27] The equation shows that in the thermodynamic limit ρ^* and ρ^t become essentially identical. In other words, the points where a bubble becomes at least metastable for the first time and where the bubble becomes fully stable for the first time occur within an infinitesimal interval of densities about ρ^*. According to Eq. (11), ρ^* also gets infinitesimally close to the coexistence liquid density ρ_l^c, as expected. Precisely at this density, however, the stability of the homogeneous phase is fully preserved, since the free energy difference between the bubble and homogeneous states at ρ^* is given by (Appendix)

$$\Delta A^* = \frac{\Delta\rho_c^2}{\chi_l}\xi_{\text{sph}}\left(\frac{V}{\xi_{\text{sph}}}\right)^{1/2}, \tag{16}$$

where the asterisk stands for a positive free energy barrier. These considerations are very much related to the essential singularity known to exist at the coexistence point in the thermodynamic limit.[36]

The free energy of the unstable state is possibly the most interesting, since it represents the nucleation barrier between the homogeneous metastable and phase separated stable states. By use of Eqs. (12) and (8), it is possible to obtain an asymptotically exact expression for the unstable state in the limit of large ρ, which reads

$$\Delta A^* = \frac{16\pi}{3}\frac{\gamma^3}{\Delta p^2(\rho)}\left\{1 + 27\frac{\xi_{\text{sph}}}{V}\left(\frac{\Delta\rho_c}{\Delta\rho}\right)^4\right\}, \tag{17}$$

where $\Delta p(\rho)$ is the Laplace pressure difference corresponding to a liquid whose density is equal to the total density of the system. This result shows that the nucleation barrier in an

NVT system is higher than that expected in a grand canonical ensemble with chemical potential $\mu(\rho)$, although the corrections will vanish in the thermodynamic limit (provided that ρ is large enough). On the other hand, the nucleation barrier may be expressed in terms of the barrier expected in a grand canonical ensemble with chemical potential set to $\mu(\rho_l)$. In that case, we find that (Appendix)

$$\Delta A^* = \frac{16\pi}{3}\frac{\gamma^3}{\Delta p^2(\rho_l)}\left\{1 - 27\frac{\xi_{\text{sph}}}{V}\left(\frac{\Delta\rho_c}{\Delta\rho}\right)^4\right\}, \tag{18}$$

i.e., in this case the free energy required in the NVT ensemble is smaller than that needed in a grand canonical ensemble. Hopefully, these equations could help correcting for finite size effects in large scale simulations.[35,37]

For the stable bubble state, an expression for the free energy relative to the nucleation barrier is not appropriate, since ΔA in this case is negative. A suitable expression is obtained by direct substitution of Eq. (13) into Eq. (8), yielding

$$\Delta A = -\frac{1}{2}\frac{V\Delta\rho^2}{\chi_l}\left\{1 - 9\left(\frac{\xi_{\text{sph}}}{V}\right)^{1/3}\left(\frac{\Delta\rho_c}{\Delta\rho}\right)^{4/3} + 9\left(\frac{\xi_{\text{sph}}}{V}\right)^{2/3}\left(\frac{\Delta\rho_c}{\Delta\rho}\right)^{8/3} + O(V^{-1})\right\}. \tag{19}$$

Note that the free energy of the stable bubble state, Eq. (19), is given in terms of deviations from the Helmholtz free energy released on phase separating into two independent bulk phases.

C. Cylindrical bubble

In the case of a cylindrical bubble under periodic boundary conditions, the length of the cylinder is equal to the box length L. Only the radius of the cylinder is left as a free parameter. The equilibrium states are obtained from Eq. (6), with $n = 1/2$ and $k_g = 2\sqrt{\pi L}$. In this case, the solutions to the Laplace equation are now the roots of a cubic polynomial [Eq. (6)]. Not surprisingly, the most relevant qualitative features observed previously in the spherical case are also observed in this case, the main differences arising from the actual value of the relevant exponents. For this reason, we only present a brief summary of the most relevant results.

In analogy to the case of a spherical bubble, a cylindrical bubble cannot be stabilized until the overall liquid density is smaller than a threshold density ρ^*:

$$\rho^* = \rho_l^c + 3\Delta\rho_c\left(\frac{\xi_{\text{cyl}}}{V}\right)^{2/9} \quad \text{with } \xi_{\text{cyl}} = \frac{\pi^{3/2}}{8}\frac{\gamma^3\chi_l^3}{\Delta\rho_c^6}. \tag{20}$$

Note that the above equation is expressed in terms of a characteristic volume depending on the fluid properties only.

The total density at which the stable cylindrical bubble becomes absolutely stable relative to the homogeneous system is given by

$$\rho^t = \rho^* + 3(2^{1/3}-1)\Delta\rho_c\left(\frac{\xi_{\text{cyl}}}{V}\right)^{2/9}. \tag{21}$$

For densities far larger than ρ^*, the energy barrier may be expressed in terms of deviations away from the nucleation energy in an open system of density ρ:

$$\Delta A^* = \frac{\pi L \gamma^2}{\Delta p^2(\rho)}\left\{1 + 2\left(\frac{\xi_{\text{cyl}}}{V}\right)^{2/3}\left(\frac{\Delta\rho_c}{\Delta\rho}\right)^3\right\}. \tag{22}$$

The result would appear to imply that the nucleation barrier is larger in a finite system size than that in an open system at equal density. On the contrary, relative to the nucleation barrier expected for an open system whose density is equal to that of the liquid in equilibrium with the bubble, the nucleation barrier is smaller:

$$\Delta A^* = \frac{\pi L \gamma^2}{\Delta p^2(\rho_l)}\left\{1 - 2\left(\frac{\xi_{\text{cyl}}}{V}\right)^{2/3}\left(\frac{\Delta\rho_c}{\Delta\rho}\right)^3\right\}. \tag{23}$$

Below ρ^t, we find that the free energy difference between the homogeneous fluid and stable cylindrical bubble is

$$\Delta A = -\frac{1}{2}\frac{V\Delta\rho^2}{\chi_l}\left\{1 - 8\left(\frac{\xi_{\text{cyl}}}{V}\right)^{1/3}\left(\frac{\Delta\rho_c}{\Delta\rho}\right)^{3/2}\right.$$
$$\left. + 4\left(\frac{\xi_{\text{cyl}}}{V}\right)^{2/3}\left(\frac{\Delta\rho_c}{\Delta\rho}\right)^3 + O(V^{-1})\right\}. \tag{24}$$

Note also that the free energy of the stable cylindrical bubble shows exactly the same system size dependence as that of the spherical bubble [cf. Eqs. (19) and (24)].

D. Tetragonal bubble (slab)

In this case, we consider a state where the vapor extends throughout the box in two directions, forming a tetragon (or slab) of fixed surface area, $2L^2$, surrounded by the liquid phase. The situation here is very simple, because the exposed surface area does not depend on the volume of the slab, so $n=0$ and $k_g=2L^2$. Furthermore, since the surface is flat, the only possible equilibrium state is that where both the liquid and vapor phases have equal pressures. Therefore, the density of the liquid in equilibrium with the bubble is $\rho_l=\rho_l^c$, independent of ρ. As long as the two resulting interfaces are sufficiently far away such that their interaction is negligible, any such state is at least partially stable. The free energy released in the transition is given by

$$\Delta A = -\frac{1}{2}\frac{V\Delta\rho^2}{\chi_l}\left\{1 - \left(\frac{\xi_{\text{slb}}}{V}\right)^{1/3}\left(\frac{\Delta\rho_c}{\Delta\rho}\right)^2\right\} \quad \text{with } \xi_{\text{slb}} = \frac{64\gamma^3\chi_l^3}{\Delta\rho_c^6}. \tag{25}$$

Within the approximations introduced in Sec. II A 2, Eq. (25) is exact and contains no higher order terms, unlike Eqs. (19) and (24), which are only the asymptotically exact results. Note once more that the system size dependence is the same as that in the cases of spherical and cylindrical bubbles. From Eq. (25), we find that the slab state will be absolutely stable relative to the homogeneous state for densities smaller than

$$\rho^t = \rho_l^c + \Delta\rho_c\left(\frac{\xi_{\text{slb}}}{V}\right)^{1/6}. \tag{26}$$

E. Crossover regimes

In Secs. II B–II D, we have found that spherical (sph), cylindrical (cyl), and slablike (slb) bubbles may become stable relative to the homogeneous stretched liquid. However, at a given density ρ, only the state of lowest free energy will be observed. In order to determine exactly which state has the lowest free energy, we need to compare Eqs. (19), (24), and (25). As noted previously, to first order, all of these equations show the same system size dependence, and accordingly, the crossover regime is system size independent. Comparison of the mentioned equations shows that a transition from spherical to cylindrical bubble is expected for $|\Delta\rho| > (4\pi/3^4)|\Delta\rho_c|$, while a transition from cylinder to slab is expected for $|\Delta\rho| > |\Delta\rho_c|/\pi$. A transition from a spherical bubble to a slab is also possible if $|\Delta\rho| > 1/3(2/\pi)^{1/2}|\Delta\rho_c|$, but this condition is fulfilled well after the transition to a cylinder has occurred.

Interestingly, the conditions obtained for the first order approximation are exactly those determined by simple geometrical arguments, that is, by considering that the transition occurs for that domain with smallest surface area, such that any curvature effect on the vapor pressure may be ignored.[6,24,38] In order to reveal the system size dependence of the transitions, we need to consider second order corrections to the free energy. For the crossover from spherical to cylindrical bubbles, calculation of sufficiently accurate transition densities requires solving a polynomial of order 10. Fortunately, we can obtain solutions in the limit of large system sizes (Appendix). The asymptotically exact result for the spherical to cylindrical transition is

$$\Delta\rho = \frac{4\pi}{81}\Delta\rho_c\left\{1 - \frac{(28)(243)}{(152)(243) + 256((4\pi/3)(V/\xi_{\text{sph}}))^{1/3}}\right\}^{-6}. \tag{27}$$

For the crossover from cylinder to slab geometries, the transition density is obtained as the root of a cubic equation. The asymptotically exact solution reads as follows:

$$\Delta\rho = \frac{1}{\pi}\Delta\rho_c\left\{1 - \frac{4\pi^{3/2}}{12\pi^{3/2} + 8(V/\xi_{\text{cyl}})^{1/3}}\right\}^{-2}. \tag{28}$$

Finally, for the crossover from spherical to slab geometries, the transition density is obtained as the solution of a simple quadratic equation. With the same level of approximation used to obtain the previous crossovers, we find that the transition occurs at

$$\Delta\rho = \frac{1}{3}\sqrt{\frac{2}{\pi}}\Delta\rho_c\left\{1 - \frac{(81)(81\pi^2)^{1/3}}{(2)(81)(81\pi^2)^{1/3} + 4^{1/3}(V/\xi_{\text{sph}})^{1/3}}\right\}^{-3/2}. \tag{29}$$

In all cases, the region where the cavitated domains are most stable increases with system size towards their asymptotic value. Furthermore, the large magnitude of the exponents of the bracketed term indicates that the corrections can be fairly

TABLE I. Table showing the different possible stable states that can be found as a function of system size (hom, homogeneous state; sph, spherical bubble state; cyl, cylindrical bubble state; slb, slablike state). The first column indicates the range of volumes where each sequence of transitions may be observed, and the third column illustrates the actual sequence observed in that range. Assuming bubble formation, the arrows indicate decreasing system density. Note that the crossover from one regime to the other occurs for volumes actually several orders of magnitude larger than ξ_{sph}, as explicitly indicated in the second column.

Volume range	Order of magnitude	Stable domains observed
$\dfrac{V}{\xi_{sph}} > \dfrac{4^3}{\pi^4}\left(\dfrac{4}{3}\right)^{41}$	$\dfrac{V}{\xi_{sph}} > 9 \times 10^4$	$\text{hom} \to \text{sph} \to \text{cyl} \to \text{slab}$
$\dfrac{4^3}{\pi^4}\left(\dfrac{4}{3}\right)^{41} < \dfrac{V}{\xi_{sph}} < \dfrac{\pi^5}{2^7}\left(\dfrac{3}{2}\right)^{22}$	$9 \times 10^4 < \dfrac{V}{\xi_{sph}} < 2 \times 10^4$	$\text{hom} \to \text{cyl} \to \text{slab}$
$\dfrac{\pi^5}{2^7}\left(\dfrac{3}{2}\right)^{22} < \dfrac{V}{\xi_{sph}} < \dfrac{3^4 2^7}{\pi}$	$2 \times 10^4 < \dfrac{V}{\xi_{sph}} < 3 \times 10^3$	$\text{hom} \to \text{slab}$
$\dfrac{V}{\xi_{sph}} < \dfrac{3^4 2^7}{\pi}$	$\dfrac{V}{\xi_{sph}} < 3 \times 10^3$	hom

large already to second order. Therefore, we cannot rule out that the sequence of transitions expected from the infinite limit analysis is altered due to system size effects. However, to this level of accuracy, comparison of Eqs. (27) and (29), in the unrealistic limit of $V \to 0$, shows that the transition to a cylinder is predicted to occur before the transition to a slab regardless of system size.

Actually, Eqs. (27)–(29) are only asymptotically correct solutions, obtained from asymptotically correct free energies [Eqs. (19), (24), and (25)]. To assess the order in which the possible transitions occur for small system sizes, it is safer to compare the transition densities [Eqs. (15), (21), and (26)] between homogeneous and cavitated states. These are (mathematically) exact results of the approximate model free energy [Eq. (9)]. Also, we must consider that the transition from a homogeneous to a cavitated domain must occur for a total density $|\Delta\rho|$ smaller than $\frac{1}{2}|\Delta\rho_c|$, since we expect that it should occur before $\mu(\rho)$ has actually crossed the $\mu = \mu_c$ axis.

Taking the above considerations into account we find an interesting scenario in which the succession of possible transitions changes gradually as the system size is increased, starting from a very small system size, where no cavitated domains are formed at all, to the largest system size, where spherical, cylindrical, and slablike bubbles are formed successively. This kind of behavior was also observed in two dimensional systems, although the possible domains formed in that case are the slab (or strip) and the sphere (or circle). In particular, Mayer and Wood found that for small enough systems, no stable phase-separated domain is ever formed.[6]

A summary of the different series of transitions that occur as a function of system size is presented in Table I. Note that the full suite of transitions $\text{hom} \to \text{sph} \to \text{cyl} \to \text{slb}$ expected in the thermodynamic limit will only occur for large enough volumes, as indicated in the table. It is only above this volume that the asymptotically exact transition densities [Eqs. (27)–(29)] remain qualitatively correct.

F. Numerical calculations

Up to now, we have obtained exact or asymptotically exact expressions for the approximate free energy of Eqs. (8) and (9). The approximations that have been invoked refer to the surface of tension and to the equation of state. Although these approximations are clearly rather crude at a quantitative level, we expect them to be fairly reasonable at a qualitative level.

However, in order to test whether the adsorption at the surface of tension is actually negligible, and whether the capillary approximation holds at a quantitative level, we must address two important issues. The first one refers to the effect of fluctuations,[17] which needs to be taken into account at least at a rudimentary level.[23,25,26] The second issue refers to the use of accurate thermodynamic data for the equation of state and surface tension. In previous works, this has been found to be necessary if quantitative agreement is sought.[24,26,39]

In order to account for fluctuations at a rudimentary level, we calculate the chemical potential as an average over all possible states,

$$\langle \mu(\rho) \rangle = \frac{\sum_i^{\Lambda} \mu_i e^{-\beta \Delta A_i}}{\sum_i^{\Lambda} e^{-\beta \Delta A_i}}, \tag{30}$$

where $i \in \Lambda$ and $\Lambda = \{\text{hom}, \text{sph}, \text{cyl}, \text{slb}\}$. A more sophisticated approach would involve summing over all possible states on the free energy surface, that is to say, over all possible values of the geometric parameters (sphere radius, cylinder radius, slab width), as suggested by Reguera et al.[25]

Since we will compare the above model to simulation data for the Lennard-Jones fluid, we will need to suplement it with an accurate equation of state. Unfortunately, the theoretical expressions available[40–42] are not accurate enough for our purposes, and we will employ a modified Benedict-Webb-Rubin (MBWR)-type parametric fit to simulation data. Among the three equations of state of this type known to us for the Lennard-Jones fluid,[43–45] we have chosen that of Sun and Teja because it was found to perform best inside the coexistence region. The reason is that these authors imposed the exact first five virial coefficients in their fit. In order to account for the effect of potential truncation, the actual MBWR equation of Sun and Teja is modified with corrections proposed by Johnson et al.[44]

Once we have considered how to deal with fluctuations and quantitative equation of state effects, we can test the capillary drop model, Eq. (1), in the following way. For a chosen fixed density ρ, we solve Eq. (2) for the chemical potential, taking into account the constraint of fixed number of particles and using the MBWR equation of state to predict the Laplace pressure difference $\Delta p(\mu)$. The surface tension required in the Laplace equation is taken from our own simulations, as determined by Binder's method.[38] We will henceforth refer to the simple fluctuation model as the many-state capillary drop (MSCD) model in analogy to the two-state capillary drop model considered in a previous work.[26]

III. MODEL AND SIMULATIONS

To test the predictions of the previous section, we have performed a computer simulation study of the Lennard-Jones fluid. Molecules interact with each other through a pairwise potential of the form

$$U_{LJ}(r) = 4\epsilon \left\{ \left(\frac{\sigma}{r} \right)^{12} - \left(\frac{\sigma}{r} \right)^{6} \right\}, \qquad (31)$$

where ϵ is the well depth and σ is the molecular diameter. The potential is truncated and shifted at $r_c = 4\sigma$ and no long range corrections are employed. Being concerned with inhomogeneous states, the standard long range corrections, based on a uniform density approximation,[7] are not appropriate. Unless noted otherwise, we will use reduced Lennard-Jones units in our discussion.

In order to obtain subcritical isotherms, we perform grand canonical Monte Carlo simulations. The outcome of the simulations is the probability, $\Pi(N; \mu_0, V, T)$, of observing N particles inside a volume V at a chosen temperature T and chemical potential μ_0. If the distribution spans a sufficiently large range of particle numbers, the whole equation of state, $\mu = \mu(\rho)$, ranging from dilute vapor states to dense liquid states can be obtained,[26,27,46] and the surface of tension of the flat interface may be determined.[38] The accurate computation of such broad distributions is not a trivial task, especially for large system sizes,[38,47,48] but several powerful techniques may be employed.[24,27,49–55] In this work, we employed grand canonical transition-matrix Monte Carlo (TMMC) to calculate the particle number probability distribution $\Pi(N; \mu_0, V, T)$. The reader is referred to Refs. 27 and 56–58 for further details on this technique.

Prior to the study of droplet and bubble formations, the coexistence chemical potential needs to be determined. This is usually done by employing the "equal area rule," which implies a reweighting of the distributions such that the areas below the vapor and liquid peaks are the same.[27,46,51,53,59] Alternatively, the coexistence chemical potential may be determined with no need for reweighting by looking for the intersection point in the chemical potential-pressure plane. This is a convenient method, because knowledge of $\Pi(N; \mu_0, V, T)$ allows for the calculation of pressure differences without explicit evaluation of the virial.[27,46] Figure 1 shows such a plot for $T = 0.85$ and system sizes $L = 8.020$, 12.030, and 16.040. The curve with small positive slope corresponds to the bulk vapor phase, while that with the steep
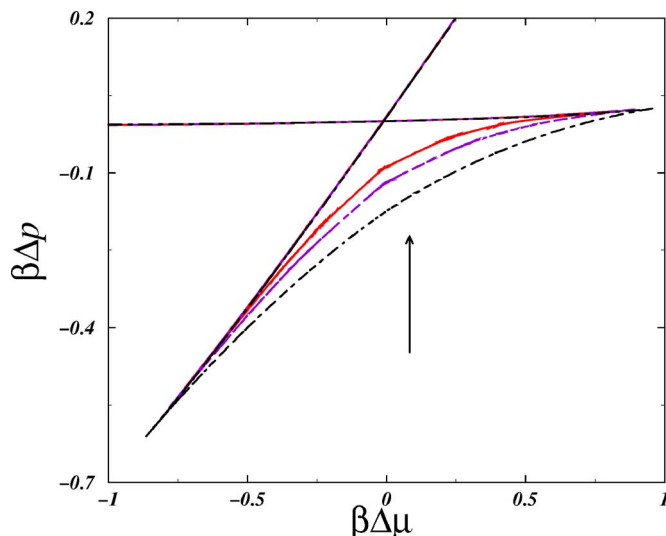

FIG. 1. Pressure vs chemical potential isotherms for systems of different sizes at $T = 0.85$. The chemical potential and pressure are expressed as $\Delta\mu = \mu - \mu_0$ and $\Delta p = p - p_0$, where $p_0 = p(\mu_0, T)$ and $\mu_0 = -9.725\,009\,9$ is the chemical potential employed during the grand canonical simulations. Full line, $L = 16.040$; dashed line, $L = 12.30$, and dot-dashed line, $L = 8.020$. The arrow points in the direction of increasing system size.

positive slope corresponds to the bulk liquid phase. These two branches intersect at a point where both the pressure and chemical potential are equal. For sufficiently large systems, the branch with negative curvature is that region where two phase states have lower free energy than the bulk phases. The cusps or *spina* signal the limits of stability of the bulk phase. In Table II, we compare coexistence chemical potentials obtained from the equal area rule and the p-μ plot for a number of temperatures and system sizes. The results suggest a small system size dependence of the coexistence chemical poten-

TABLE II. Coexistence chemical potentials as obtained from the equal area rule and the pressure-chemical potential intercept for the different system sizes and temperatures considered in this work. First column: system size; second column: temperature; third column: coexistence chemical potential from equal area rule; fourth column: coexistence chemical potential from pressure-chemical potential intercept.

| L	T	μ_c^{ea}	μ_c^{pm}
8.0192	1.10	−11.5736	−11.5726
12.0289	1.10	−11.5739	−11.5731
16.0385	1.10	−11.5737	−11.5736
8.0192	1.00	−10.8033	−10.8019
12.0289	1.00	−10.8035	−10.8032
16.0385	1.00	−10.8038	−10.8036
8.0192	0.90	−10.0790	−10.0773
12.0289	0.90	−10.0790	−10.0785
16.0385	0.90	−10.0770	−10.0768
8.0192	0.85	−9.7356	−9.7338
12.0289	0.85	−9.7357	−9.7352
16.0385	0.85	−9.7361	−9.7359
8.0192	0.75	−9.0945	−9.0924
12.0289	0.75	−9.0936	−9.0923
16.0385	0.75	−9.0100	−9.0997
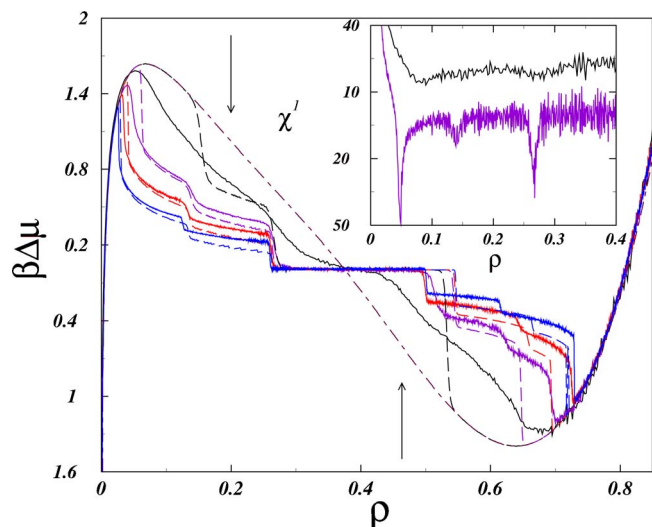
FIG. 2. Chemical potential vs density isotherms for systems of different sizes at $T=0.75$. The chemical potential is measured relative to the coexistence chemical potential. The full lines are simulation results, the dashed lines are results from the many-state model, and the dot-dashed line is the mean-field parametric equation of state. The inset shows the inverse susceptibility for the two smallest system sizes. Units are arbitrary and results have been shifted vertically for clarity. The system sizes studied are $L=21.010$, $L=16.040$, $L=12.30$, and $L=8.020$. The arrows point in the direction of increasing system size.

tials, with a faster convergence for the equal area rule. A small difference of order $1/V$ between both methods is expected from simple arguments.[46]

IV. COMPARISON BETWEEN THEORY AND SIMULATION

A. Qualitative test of the theory

Having determined the coexistence chemical potentials, let us now consider whether the previous theoretical analysis qualitatively grasps the different possible transitions that could occur within the two phase region.

Figure 2 presents computed $\mu=\mu(\rho)$ isotherms for different system sizes at temperature $T=0.75$. Focusing first on the largest system size considered, $L=21.010$, we note several (smoothed) discontinuities as the density increases from the undersaturated vapor to the compressed liquid. First, a very conspicuous discontinuity occurs somewhat above the coexistence vapor density. At that point, the equation of state changes abruptly and becomes a decreasing function of density. The nature of the "unstable" character of the points in the curve can be understood from the considerations of Sec. II. Those states are unstable as long as the system is open, for example, in a grand canonical ensemble. However, if the system is kept at constant overall density, the states with negative slope in Fig. 2 are actually stable.[9,60] It is important to point that they do differ from those other states having positive slope in one significant respect, namely, they are phase separated (inhomogeneous) states, with a majority phase surrounding some domain of the other phase. Therefore, the discontinuity observed at lowest density corresponds to a transition point where a nucleated domain becomes absolutely stable relative to the homogeneous vapor state. In this case ($L=21.010$), the domain formed is a

spherical droplet. After this transition, two other discontinuities appear before the midpoint $\frac{1}{2}\Delta\rho_c$ is reached. The one occurring at intermediate supersaturated states corresponds to a transition from spherical to cylindrical domains, while the last one occurring at highly supersaturated states corresponds to a transition between the cylindrical and slablike states.[61] The latter have a particular feature, namely, they correspond to states with zero slope. Since the slab has a flat interface, it can only occur for those states where the chemical potential of both phases is equal to the coexistence chemical potential (see the Laplace equation).

Once the midpoint is crossed, a sequence of transitions analogous to that described above occurs in reverse order, the only other difference being that the majority phase is then the liquid phase, and the domains formed are no longer droplets but bubbles. Actually, the isotherms are roughly antisymmetric with respect to the midpoint: all the theoretical description performed previously for states with liquid phase as the majority phase hold just as well for states with vapor phase as the majority phase, provided the labels v and l are interchanged.

In Fig. 3, we present a series of snapshots obtained during the course of the simulation of the largest system, with $L=21.010$. Each of the snapshots was sampled from a different density interval, corresponding to the different regimes expected: homogeneous vapor, spherical droplet, cylindrical droplet, slab, cylindrical cavity, spherical cavity, and homogeneous liquid. Visual inspection of the snapshots shows that, indeed, the states observed correspond to those predicted by the capillary theory of Sec. II in the limit of large system sizes, thus justifying the preceding discussion.

Taking now into consideration the other system sizes studied at $T=0.75$, namely, $L=16.04$, $L=12.03$, and $L=8.02$, we note that the first two show the same series of transitions as the largest system. Several other qualitative results from the theory can also be verified by looking at the isotherms of the three largest system sizes of Fig. 2.

- The hom$\rightarrow$sph transition gets closer and closer to the coexistence densities with increasing system size, as predicted by Eq. (15).

- The sph$\rightarrow$cyl transition density tends asymptotically towards a constant, and the approach occurs from beyond that constant, as predicted by Eq. (27).

- The cyl$\rightarrow$slb transition density tends asymptotically towards a constant, and the approach also occurs from beyond that constant, as predicted by Eq. (28).

For the smallest system size, however, the equation of state seems to exhibit only two transitions before the midpoint, where the vapor is the majority phase, and similarly, two other transitions beyond the midpoint, where the liquid is the majority phase. In order to make the possible transitions more apparent, the inset of Fig. 2 plots the inverse susceptibilities, $\chi^{-1}=\partial\mu/\partial\rho$, for the two smallest system sizes. For $L=12.03$, the plot clearly shows three minima, corresponding to each of the geometric transitions. For the smallest system size, however, only two minima are apparent. This confirms that the smallest system size only shows
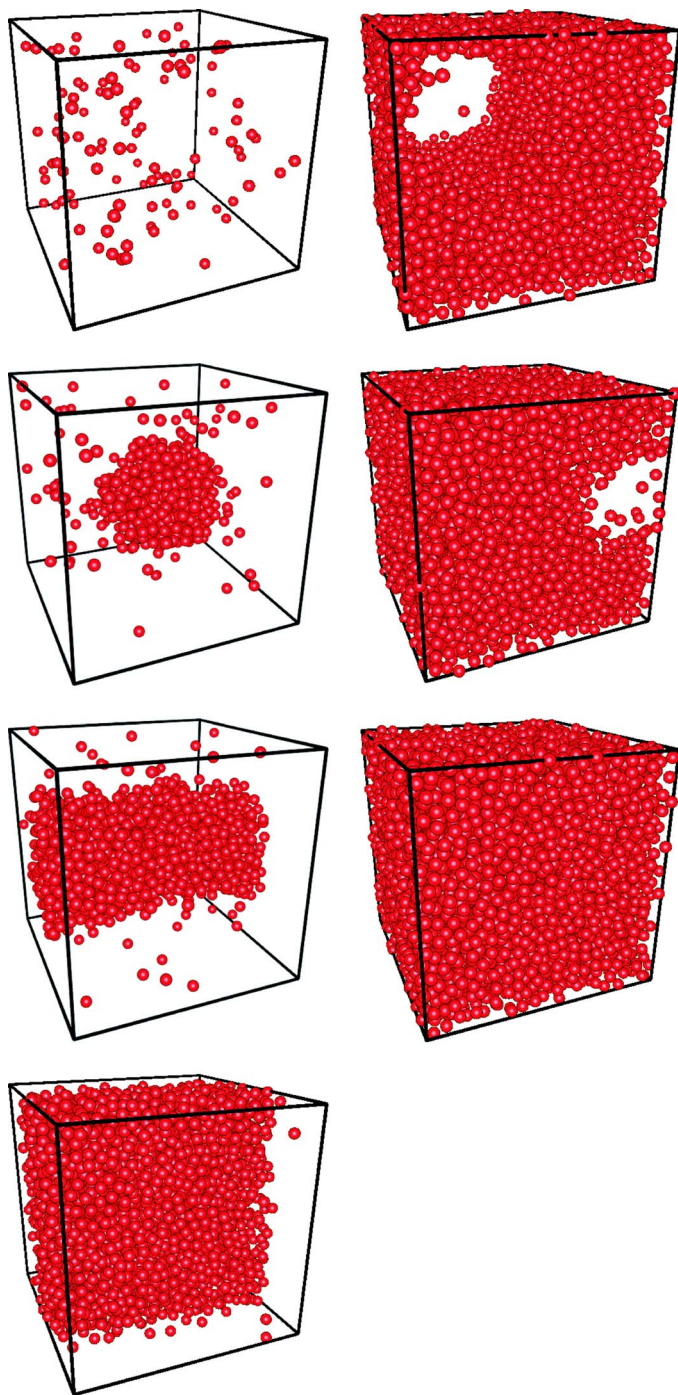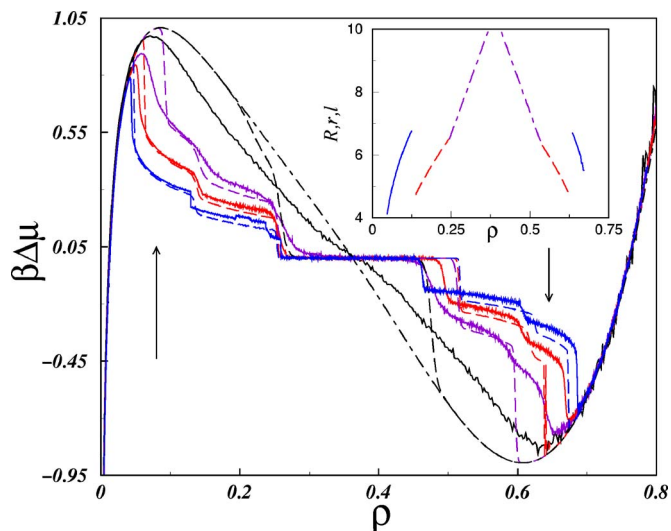
FIG. 4. Chemical potential vs density isotherms for systems of different sizes at $T=0.85$. The chemical potential is measured relative to the coexistence chemical potential. The full lines are simulation results, the dashed lines are results from the two-state model, and the dot-dashed line is the mean-field parametric equation of state. The system sizes studied are $L=21.01$, $L=16.04$, $L=12.03$, and $L=8.02$. The arrows point in the direction of decreasing system size. The inset shows the size of those domains that are stable at the given density in the $L=21.01$ system. R, r, and l denote the radii and the width of spherical (full lines), cylindrical (dashed lines), and tetragonal (dot-dashed lines) domains, respectively.

FIG. 3. A series of snapshots at $T=0.75$ and $L=21.010$, corresponding to states of increasing density.

two transitions and is consistent with expectations from Sec. II E, which predict that only two transitions occur within the interval of densities $\frac{1}{2}\Delta\rho_c$ for small enough system sizes. According to Table I, these involve a transition from the homogeneous state to the cylindrical state, followed by a second transition from cylinder to slab. These expectations are confirmed by visual inspection of stored configurations (not shown). Unfortunately, it is not meaningful to study system sizes smaller than $L=8.02$ because our model has a cutoff radius $r_c=4$.

In principle, the occurrence of other regimes could be studied by changing the characteristic volume, ξ_{sph}, i.e., by

studying isotherms at other temperatures. In Fig. 4, we present isotherms for $T=0.85$ at four different system sizes. For the smallest system size, we observe the same behavior as that found for the same system size at $T=0.75$, although the appearance of the isotherms is already much smoother, and the signature of the transition from cyl$\rightarrow$slb is here very weak. For the next system size at this temperature, the full sequence of transitions corresponding to the large system size limit is already achieved, although the discontinuities are not strongly apparent for the $L=12.02$ and $L=16.03$ systems. Only when the largest system size is considered does the sequence of transitions reveal itself as rather clear steps in the equation of state.

An undesirable but relevant issue associated with the simulation data for the largest system size ($L=21.01$) is the difficulty of proper sampling of configuration space. This issue of insufficient sampling manifests itself in the isotherm as small spurious steps close to the cyl$\rightarrow$slb transition on the vapor side, and in the cyl$\rightarrow$slb transition on the liquid side, which extend far beyond expectations. Since these transitions are all first order and have a large activation energy that increases with system size, it becomes virtually impossible to obtain good equilibrated results for large systems, as noted previously.[24,54,58]

In order to show the occurrence of the transitions in the remaining small system size regimes, we need to consider still other temperatures, such that ξ_{sph} is large enough. For our model Lennard-Jones fluid, this is achieved only close to the critical point. Using the tail correction scheme in Ref. 44, Punnathanam and Corti[62] have estimated the critical properties of the particular Lennard-Jones fluid used in this study to be $T_c=1.246$, $\rho_c=0.308$, and $p_c=0.118$. Figure 5 shows iso-
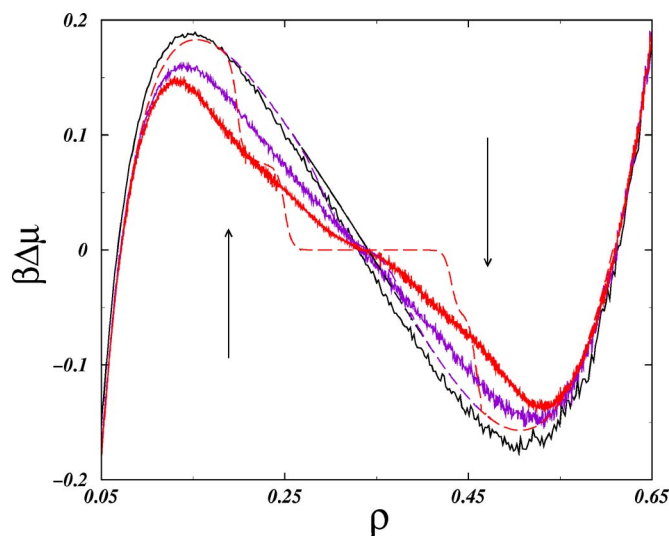
FIG. 5. Chemical potential vs density isotherms for systems of different sizes at $T=1.10$. The chemical potential is measured relative to the coexistence chemical potential. The full lines are simulation results, the dashed lines are results from the many-state model, and the dot-dashed line is the mean-field parametric equation of state. The system sizes studied are $L=16.040$, $L=12.30$, and $L=8.020$. The arrows point in the direction of decreasing system size.
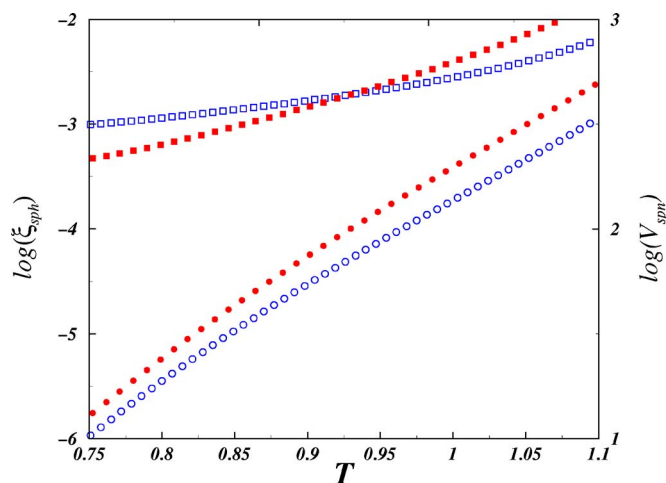

FIG. 6. Temperature dependence of some relevant volume dimensions. The empty symbols refer to the characteristic volume of spherical domain formation, ξ_{sph} (left ordinate axis). The full symbols refer to "spinodal" volumes, V_{spn}, as explained in the text. The circles refer to the condensation transition and the squares to the cavitation transition. ξ_{sph} is calculated using MBWR equation of state data, together with interpolated surface tensions as obtained from simulation. V_{spn} is calculated using Eq. (15), with coexistence and spinodal points as determined from the MBWR equation of state.

$$\xi_{sph} \propto |T - T_c|^{-3\nu}. \tag{32}$$

Note that ν is the scaling exponent governing the divergence of the correlation length. Therefore, ξ_{sph} is expected to be an increasing function of temperature, diverging at the critical point and showing exactly the same scaling behavior as the cube of the correlation length. Actually, the analogy between density fluctuations and droplet formation is at the heart of some of the hyperscaling relations.[29]

The qualitative temperature dependence predicted in the previous equation is tested numerically in Fig. 6, where we plot ξ_{sph} for both bubble and droplet formations. Within the range of temperatures considered in the simulations, ξ_{sph} indeed monotonically increases for both bubble and droplet formations. The value relevant to bubble formation is several orders of magnitude larger than that relevant to droplet formation, but as the critical temperature is approached, both characteristic volumes should become equal and strictly follow Eq. (32). Although increasing and eventually diverging, ξ_{sph} remains several orders of magnitude smaller than one molecular diameter up to $T=1.10$. Despite this, finite size effects can be significant, because they occur for volumes several orders of magnitude larger than ξ_{sph}, as noted in the captions to Table I. In order to illustrate this point, we introduce another volume scale, V_{spn}, defined as that volume where the density of the transition hom$\rightarrow$sph becomes equal to the mean-field spinodal density. If this transition were the only way the homogeneous phase could phase separate, the definition of V_{spn} would imply that any finite system of smaller volume would remain homogeneous all the way up to the mean-field spinodal (actually we do know that other relaxation mechanisms exist, but the definition is useful to illustrate the point anyway). An order of magnitude estimate of this volume may be obtained by equating Eq. (15) to the mean-field spinodal density. The results obtained are shown in Fig. 6 (ordinate axis to the right of the plot). Notice that
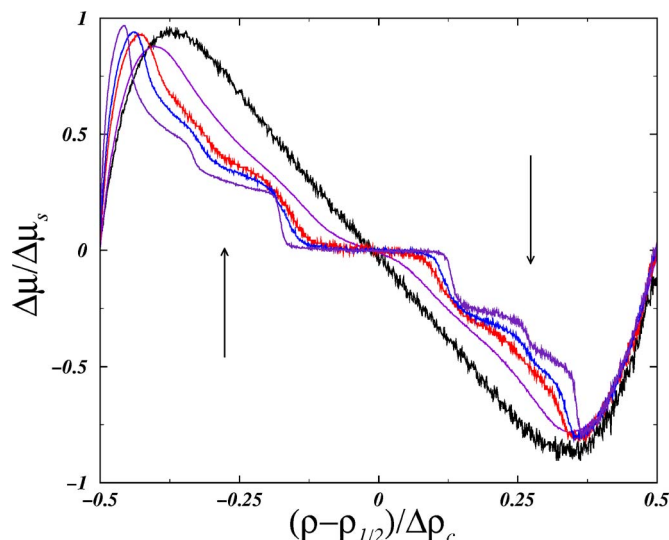
therms for systems at $T=1.10$. Indeed, in this case we find that for the smallest system size, the isotherm does not show sharp or blurred steps in the chemical potential, but rather looks very much like a smooth van der Waals loop. Actually, the computed isotherm closely resembles the parametric MBWR equation of state of Sun and Teja, all the way from the low density vapor to the liquid side and in between the mean-field spinodal points. In contrast, for the largest system size shown in the figure, the smoothed isotherm seems to exhibit two transitions involving cylindrical and slablike domains. We speculate that the intermediate system sizes exhibit only one transition, involving only homogeneous and slablike states. However, the scenarios predicted in Table I should be considered as only approximately correct, because none of the different domains apart from the homogeneous state overwhelmingly dominate over other possible states.[17]

Implicit in the above discussion is the assumption that ξ_{sph}, the characteristic volume scale governing the occurrence of the different regimes, increases with temperature. Actually, the temperature dependence of ξ_{sph} is not immediately obvious because it depends on three nontrivial temperature-dependent properties, namely, $\xi_{sph} \propto \chi^3 \gamma^3 / \Delta\rho_c^6$. A qualitative analysis based on an equation of state is therefore a difficult matter. Nevertheless, assuming that the behavior is monotonic, we can study the temperature dependence close to the critical point. In that case, the nontrivial temperature-dependent properties may be expressed as simple power laws.[29] Accordingly, the scaling form of ξ_{sph} may be expressed in terms of the scaling exponents of the isothermal compressibility, surface tension, and coexistence density difference. These three exponents are not independent, however.[29] Taking into account hyperscaling relations, the scaling of ξ may be written in its simplest possible form:

FIG. 7. A series of isotherms obtained for system size $L=12.03$ and different temperatures. The density is shifted by an amount $\rho_{1/2}=\frac{1}{2}\Delta\rho_c$ and then normalized by $\Delta\rho_c$. The chemical potential is expressed relative to the coexistence chemical potential and then normalized by $\Delta\mu_s=\mu_s-\mu_c$, with μ_s, the (vapor) mean-field spinodal point as determined by the MBWR equation of state. The arrows point in the direction of increasing temperature.

the temperature dependence of $V_{\rm spn}$ is very similar to that of $\xi_{\rm sph}$, and $V_{\rm spn}$ spans several orders of magnitude over the temperature range investigated. For the cavitation transition at a temperature of $T=1.10$, we find $V_{\rm spn}=2200\sigma^3$ corresponding to linear dimensions of about $L=13\sigma$.

Note that the suite of transitions that the system is expected to show depends on the ratio $V/\xi_{\rm sph}$. Since $\xi_{\rm sph}$ is an increasing function of the temperature, this ratio will increase monotonically, whether the temperature is kept constant and V increased, or V left constant and T decreased. Hence, the same crossover sequence as observed previously by increasing V at fixed T is expected to occur by decreasing the temperature at constant volume. Figure 7 shows a set of isotherms obtained for several temperatures at fixed system size $L=12.03$. In order not to upset the comparison and have all the data fit into a similar scale, the plot shows scaled chemical potentials and densities. We emphasize that this variable reduction does not change the behavior of the isotherms, but only the scale. Inspection of the figure shows that the computed isotherms closely follow the theoretical predictions. At the highest temperature, the isotherm resembles a mean-field van der Waals-type loop, as expected in the limit of small system sizes, while at the lower temperatures, the loops display the (smoothed) suite of discontinuities observed for large system sizes.

B. Quantitative test of the capillary model

Along with the computed isotherms, Figs. 2, 4, and 5 include as dashed lines the predictions of the MSCD model. The overall agreement is seen to be quite reasonable. In particular, for large systems and low temperatures, the predictions of MSCD closely follow the simulation results, although better so for the vapor side than the liquid side. Possibly, curvature effects on the surface tension are more important for bubbles than for droplets. It has been shown

that fairly small droplets already exhibit tensions rather close to that of the flat interface, and that the Tolman length is small,[11,31,39,63,64] but analogous tests for bubbles have not been performed. Intriguingly, the agreement is usually much better for true spherical droplets than for the cylinders, although the curvature of the latter is actually smaller. In the absence of other evidence, one could hypothesize that the surface adsorption of the cylindrical domains is larger, but there is no clear reason why should that be so. The inset of Fig. 4 shows the size of those domains which are stable at the given density, for a cubic simulation box with $L=21.01$. The size is measured by means of the radii, for spherical and cylindrical domains, and the width, for the slab. Clearly, the capillary model is working for rather small domains, with size just a few molecular diameters in length.

For smaller system sizes and higher temperatures, the agreement is not as good, and the transitions are sometimes predicted to occur beyond the mean-field spinodal. Clearly, even if such predictions were fortuitously correct at a mean-field level, we should expect very large fluctuations to occur in that case.[17] The simplicity of the MSCD can hardly grasp such effects. Strikingly, when the systems are so small that no condensation occurs at all, the simulated isotherms are in very good agreement with the mean-field MBWR equation of state employed as input for the MSCD. This observation suggests that extension of the mean-field equation of state inside the two phase region is indeed significant. It describes the behavior of the fluid when the system is sufficiently small. This might also be true close to the critical point (an analysis of the droplet transition close to the critical point may be found in Ref. 23). Since $\xi_{\rm sph}$ diverges there, expectations based upon the drop model employed here would suggest that infinitely large systems are required to actually observe explicit phase coexistence. Nevertheless, ordinary mean-field equations of state would fail to describe qualitatively the conjectured loop, but an analytical expression could suffice.[65]

C. Significance of the finite size transition densities

We would now like to address a puzzling issue, dealing with the extrema of the finite size equilibrium loops obtained from simulation, the mean-field spinodal point, and their relation to a hypothesized limit of stability. We will see that the problem is mainly one of vocabulary.

Usually, it is considered that the van der Waals loop typical of an analytical equation of state is an artifact stemming from the mean-field character of statistical thermodynamic theories. The usual flat isotherms observed in most experimental situations are considered as the thermodynamically meaningful equilibrium isotherms. The continuous extrapolations of the equation of state beyond the coexistence densities into the liquid-vapor coexistence dome, which are sometimes achieved in careful experiments, are considered to correspond to metastable states. This scenario is characterized by two sets of system-size-independent properties. The first set, and experimentally most meaningful, corresponds to the phase-coexistence densities, defined here as those densities such that the liquid and vapor phases have equal chemi-
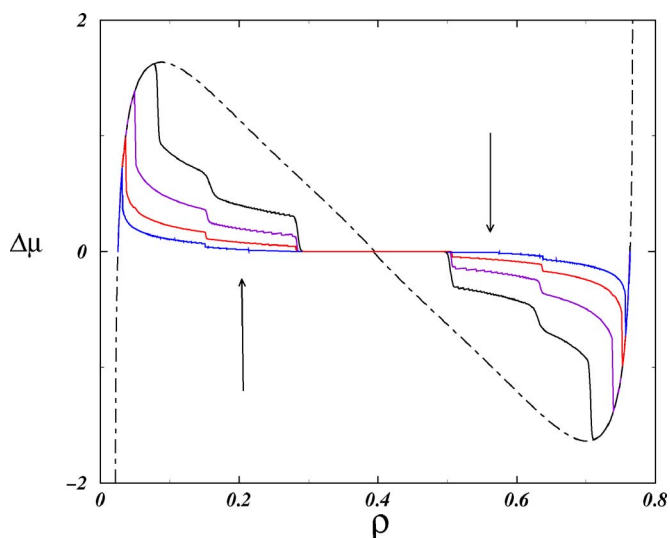
FIG. 8. Chemical potential vs density isotherms for large system sizes as predicted by the MSCD model. The isotherms were calculated for $T=0.75$ and several system sizes up to $L=100$. Because of numerical reasons, the calculations for the liquid side and large system sizes become difficult. For this reason, we have calculated the isotherms on the vapor side only. The full loop was obtained assuming the antisymmetric property of the chemical potential. The arrows point in the direction of decreasing system size.

cal potential and pressure. The second set corresponds to the mean-field spinodals, defined here as the extrema of the mean-field loops.

Contrary to this scenario, our simulations clearly show a strong finite size dependence and lead to open questions about standard knowledge of phase transitions and stability.

(1) Given that the finite size isotherms are true equilibrium states, are the extrema the actual limits of thermodynamic stability?

(2) Given that the extrema of the finite size isotherms are system size dependent, is there a meaningful system-size-independent spinodal point?

In order to resolve this apparent conflict, it is useful to plot a sequence of finite size isotherms as $V/\xi_{sph} \to \infty$. Obviously, obtaining such isotherms by means of computer simulations is unfeasible, but we can nevertheless employ the MSCD model, which was previously found to work very accurately. In Fig. 8 we plot a series of isotherms for increasing system sizes at $T=0.75$. The plot illustrates the relation between the intriguing finite size loops and the standard flat isotherm of an experiment. As the system size increases, the isotherms gradually flatten, and the extrema of the equilibrium curves approach the coexistence point asymptotically [see Eq. (15)]. One could call such points spinodals. They are the extrema of an equilibrium isotherm, and they correspond to "spina" in the p-μ plane (see Fig. 1). However, this could be misleading. Indeed, the states between the coexistence densities and the extrema are stable, not metastable. In fact, those points are the actual finite size *dew and bubble points* where the free energy of the phase separated state (vapor+droplet) first becomes lower than that of the homogeneous state. The dew and bubble points are system size dependent [see Eq. (15)], while the coexistence vapor and

liquid densities may be defined as the asymptotic thermodynamic limits of such points. For example, for the coexistence vapor density, we could write

$$\rho_v^c = \lim_{V \to \infty} \rho^t(V),\tag{33}$$

where we have used the notation of Sec. II for dew point, or transition density (we refer to a transition between a homogeneous vapor state and an inhomogeneous droplet state). Thus, the extrema of the equilibrium finite size loops correspond to limits of *full thermodynamic stability*. In the large system size limit, they will no longer appear as smooth analytical extrema, but as nonanalytical discontinuities as is expected for the system-size-independent coexistence points.[26]

On the other hand, in the limit of large system sizes, the mean-field spinodal is indeed a limit of *precarious metastable thermodynamic stability*. This can be understood by considering the free energy barrier separating the homogeneous state and the inhomogeneous state at the threshold point (this will only differ by constant factors with the barrier observed at the transition density). Inspection of Eq. (16) shows that this barrier scales as $V^{1/2}$ and is therefore infinitely large in the thermodynamic limit.[36] For this reason, homogeneous states can survive well beyond the dew and bubble points for a long time, despite the fact that the inhomogeneous spherical droplet state is more stable. In this case, they are indeed truly metastable states, which will eventually decay. Therefore, the mean field spinodal point is then meaningful as a limiting point for the occurrence of these metastable states. For small enough systems, our results show that such states can indeed be reached up to almost the spinodal point. (See Fig. 5, but recall for this small system size that those states are stable!)

V. CONCLUSIONS

In this work we have studied the behavior of subcritical isotherms in small systems under periodic boundary conditions for a temperature range spanning from slightly above the triple point to just below the critical point and for system sizes ranging from about 8 to 21 molecular diameters in lateral size (see Table II). We have found that isotherms in the chemical potential-density plane exhibit different shapes depending on the scaled system size V/ξ, where ξ is a temperature-dependent characteristic volume scale (see Table I). In the region where the vapor is the majority phase, the following four scenarios are possible (a similar situation holds for the region were the liquid is the majority phase, with cavities instead of droplets forming).

- For large system sizes, four different states are observed successively inside the coexistence region as the density is increased (see Fig. 3). At low densities, a fully homogeneous vapor state is found. As the density is increased, a state with a spherical droplet becomes more stable. Further increasing the density results in the formation of a cylindrical droplet whose sides are connected via the periodic boundary conditions of the simulation cell. Finally, at larger densities a tetragonal

slab is stabilized. The transitions between these states are responsible for the discontinuities observed in the isotherms obtained from simulation.

- For intermediate system sizes, the spherical droplet state is suppressed, and only three different states are observed, the homogeneous vapor, the cylindrical bubble, and the slab.

- For small systems, the cylindrical droplet is also suppressed, and a single transition between the homogeneous vapor and the slab is encountered.

- For very small system sizes, a condensed domain is never formed and a smooth van der Waals-type isotherm is found.

The parameter ξ, which is a function of the surface tension, compressibility, and coexistence densities, increases with temperature (see Fig. 6) and scales like the correlation length [see Eq. (32)]. Accordingly, the four possible scenarios described above can also be observed at constant volume, while varying temperature (see Fig. 7). Close to the triple point ($k_B T/\epsilon = 0.75$), systems with a lateral size as small as $L = 8\sigma$ were found to show intermediate-size-regime behavior (see item 2 above), while for $L = 12\sigma$, the large-system-size-limiting behavior was already reached (see Fig. 2). On the contrary, close to the critical point, systems as large as $L = 16\sigma$ had not yet reached the large system size behavior (see Fig. 5). It is important to point out that the geometry of the different domains and the suite of transitions are specific to the boundary conditions employed in this work. However, the importance of the Laplace effects and the nature of the condensation or cavitation transition is general and is relevant to the study of phase transitions in pores. Particularly, our results show that finite size corrections to the Helmholtz free energy barriers (appropriate for closed systems) are given as powers of the inverse volume [see Eqs. (17) and (22)].

By employing an accurate mean-field equation of state and surface tension values obtained from simulation, we find that the capillary drop model is able to predict isotherms in the chemical potential versus density plane that are in reasonable agreement with simulation. This is a remarkable result because the sizes of the domains are of molecular size. As observed in Figs. 2 and 4, this is the case at low temperatures ($T/T_c < 0.8$) and for large system sizes ($L > 16\sigma$). For example, at $k_B T/\epsilon = 0.85$ and a system size $L = 21\sigma$, where our calculations provide a very good description of the simulated isotherm (see. Fig. 4), we find spherical droplets with radii between 4.2σ and 6.5σ, cylindrical droplets with radii between 4.8σ and 6.6σ, and slabs of width between 6.5σ and 10σ. On the other hand, for small system sizes ($L \sim 8\sigma$) close to the critical point ($k_B T/\epsilon = 1.1$), where inhomogeneous states are not stable, we find that the simulated isotherms closely resemble the predictions of a mean-field equation of state, as in the van der Waals theory (see Fig. 5).

Finally, we discuss an important conceptual difference between "apparent" or "effective" system-size-dependent spinodal points, here defined as the extrema of the finite size equilibrium isotherms, and mean-field spinodal points. The former are actually system-size-dependent dew and bubble points, separating the region where homogeneous, supersaturated, or stretched fluids are thermodynamically stable from the region where such states are only partially stable. In the thermodynamic limit, the system-size-dependent dew and bubble points exhibit a nonanalytic discontinuity and coincide with the coexistence points (see Fig. 8). Only then are all states between the coexistence points and the mean-field spinodals truly metastable.

ACKNOWLEDGMENTS

APPENDIX: ALGEBRAIC MANIPULATIONS

In order to solve for the equilibrium condition we introduce an auxiliary function, whose roots are equal to those of Eq. (6),

$$f(x) = x^q - x^{q-1} + K_n, \tag{A1}$$

where $q = (2-n)/(1-n)$ amounts to 4 for spherical bubbles, 3 for cylindrical bubbles, and 2 for slab geometry and K_n is a positive constant ranging from 0 to ∞. The extrema of f obey

$$x^{q-2}(qx - (q-1)) = 0. \tag{A2}$$

The only nontrivial solution corresponds to a minimum at $x^* = 1/(2-n)$. Substitution of this result into $f(x)$ shows that the auxiliary function has roots only for values of K_n smaller than $K_n^* = (1-n)/(2-n)^{(2-n)/(1-n)}$. $f(x)$ can thus be solved exactly for $K_n = K_n^*$ and for $K_n = 0$, where the solutions are trivially found to be 0 and 1. In particular, for K_n and x close to zero, corresponding to the stable bubble and large system sizes, we can neglect higher order terms and find right away $x \approx K_n^{1/(q-1)}$.

In order to find other asymptotic solutions, let us express x in terms of deviations away from some known root, x_0, corresponding to $K_n = K_n(x_0)$ such that $x = x_0 + \delta x$. Substitution into $f(x)$ yields, after some rearrangement,

$$A_0 \delta x^2 + B_0 \delta x + (K_n(x_0) - K_n) = 0, \tag{A3}$$

where higher order terms have been ignored,

$$A_0 = C_2^q x_0^{q-2} - C_2^{q-1} x_0^{q-3},$$

$$B_0 = C_1^q x_0^{q-1} - C_1^{q-1} x_0^{q-2}, \tag{A4}$$

and C_m^n are binomial coefficients.

Two very simple cases result for $K_n(x_0)=0$ and $K_n(x_0) = K_n^*$.

(a) $K_n(x_0)=0$ and $x_0=1$. This case corresponds to the unstable solution in the limit of large system sizes. Both coefficients are finite, but we can neglect higher order terms and obtain to first order $\delta x = -K_n/B_0$.

(b) $K_n = K_n^*$ and $x_0 = x^*$. This is the case where the system is small and the total density is close to the threshold density ρ^*. In this situation, $B_0=0$, and the asymptotic solutions are $\delta x = \pm (K_n(x_0)-K_n)^{1/2}$.

Expressions for the free energies such as Eqs. (16)–(18) are obtained by direct substitution of the extremum into Eq. (9), followed by the change of variable, $w=(1/2)(1-x)$. For the remaining free energy expressions, such as Eq. (18), we add and subtract $(1-2w)w$ from Eq. (9). The resulting equation may be simplified, since the extremum condition implies $1-2w = 2^{n-1}K_n^{1-n}w^{n-1}$, yielding

$$\Delta a(w) = (1-n)\left\{\frac{2^{n-1}}{n}K_n^{1-n}w^n\right\}\left\{1 - \frac{n}{1-n}\frac{w^{2-n}}{2^{n-1}K_n^{1-n}}\right\}. \tag{A5}$$

Since the second factor on the right hand side is actually the (reduced) surface free energy of the drop, this equation is a generalization of the statement that a critical (spherical) nucleus has 1/3 of the total surface free energy (cylindrical bubbles having 1/2 of the surface free energy and slabs, obviously, 1/1). Substitution of the corresponding extremum followed by a change of variables leads to Eq. (18).

The corrections to the asymptotic limits of crossover from spherical to cylindrical bubbles are obtained by comparing Eq. (19) to Eq. (24). A cylindrical bubble becomes relatively more stable than a spherical one when the following condition is obeyed:

$$-8gy + 4g^2y^{10} < -9f + 9f^2y^8, \tag{A6}$$

where $g=(\xi_{cyl}/V)^{1/3}$, $f=(\xi_{sph}/V)^{1/3}$, and $y=(\Delta\rho_c/\Delta\rho)^{1/6}$. Multiplying both sides by $(8/9)^{10}(g^8/f^{10})$, we find that the turning point is a root of the following tenth order polynomial:

$$f(s) = 36s^{10} - 64s^8 - Ks + K, \tag{A7}$$

where $s=(8/9)(g/f)y$ and $K=(8^{10}/9^8)(g^8/f^9)$. Since $K \sim O(V^{1/3})$, for large system sizes the lowest order terms in s dominate, leading to the trivial asymptotic solution $s_\infty=1$. The solutions for smaller volumes may be obtained as small deviations from this trivial solution. Substitution of $s=1-\delta s$ into Eq. (A7), and keeping only lowest order terms, we find $\delta s = 28/(152+K)$. Undoing all previous changes of variables, this result leads to Eq. (27). The other crossover conditions, Eqs. (28) and (29), are obtained similarly.

[1] N. Metropolis, A. W. Rosenbluth, M. N. Rosenbluth, A. N. Teller, and E. Teller, J. Chem. Phys. **21**, 1087 (1953).
[2] K. Binder, Rep. Prog. Phys. **50**, 783 (1987).
[3] W. Wood and J. D. Jacobson, J. Chem. Phys. **27**, 1207 (1957).
[4] B. J. Alder and T. E. Wainright, J. Chem. Phys. **27**, 1208 (1957).
[5] B. J. Alder and T. E. Wainright, Phys. Rev. **127**, 359 (1962).
[6] J. E. Mayer and W. W. Wood, J. Chem. Phys. **42**, 4268 (1965).
[7] M. Allen and D. Tildesley, *Computer Simulation of Liquids* (Clarendon, Oxford, 1987).
[8] M. Rao, B. J. Berne, and M. H. Kalos, J. Chem. Phys. **68**, 1325 (1978).
[9] K. Binder and M. H. Kalos, J. Stat. Phys. **22**, 363 (1980).
[10] H. Ulbricht, J. Schmelzer, R. Mahnke, and F. Schweitzer, *Thermodynamics of Finite Systems and the Kinetics of First-Order Phase Transitions* (Teubner, Leipzig, 1988).
[11] P. R. ten Wolde and D. Frenkel, J. Chem. Phys. **109**, 9901 (1998).
[12] G. E. Norman and V. V. Stegailov, Dokl. Phys. **47**, 667 (2002).
[13] P. Virnau, M. Müller, L. G. MacDowell, and K. Binder, New J. Phys. **6**, 7 (2004).
[14] J. Merikanto, H. Vehkamati, and E. Zapadinsky, J. Chem. Phys. **121**, 914 (2004).
[15] A. Luzar, J. Phys. Chem. B **108**, 19859 (2004).
[16] C. Valeriani, E. Sanz, and D. Frenkel, J. Chem. Phys. **122**, 194501 (2005).
[17] H. Furukawa and K. Binder, Phys. Rev. A **26**, 556 (1982).
[18] A. Cabañas, E. Enciso, M. C. Carbajo, M. J. Torralvo, C. Pando, and J. A. R. Renuncio, Chem. Commun. (Cambridge) **20**, 2618 (2005).
[19] A. V. Neimark, P. I. Ravikovitch, and A. Vishnyakov, J. Phys.: Condens. Matter **15**, 347 (2003).
[20] M. Pleimling and W. Selke, J. Phys. A **33**, L199 (2000).
[21] M. Pleimling and A. Hüller, J. Stat. Phys. **104**, 971 (2001).
[22] M. Biskup, L. Chayes, and R. Kotecky, Europhys. Lett. **60**, 21 (2002).
[23] K. Binder, Physica A **319**, 99 (2003).
[24] T. Neuhaus and J. S. Hager, J. Stat. Phys. **113**, 47 (2003).
[25] D. Reguera, R. K. Bowles, Y. Djikaev, and H. Reiss, J. Chem. Phys. **118**, 340 (2003).
[26] L. G. MacDowell, P. Virnau, M. Müller, and K. Binder, J. Chem. Phys. **120**, 5293 (2004).
[27] V. K. Shen and J. R. Errington, J. Phys. Chem. B **108**, 19595 (2004).
[28] A. V. Neimark and A. Vishnyakov, J. Phys. Chem. B **109**, 5962 (2005).
[29] J. Rowlinson and B. Widom, *Molecular Theory of Capillarity* (Clarendon, Oxford, 1982).
[30] A. J. Yang, J. Chem. Phys. **79**, 6289 (1983).
[31] D. J. Lee, M. M. Telo da Gama, and K. E. Gubbins, J. Chem. Phys. **85**, 490 (1986).
[32] D. Kashchiev, J. Chem. Phys. **118**, 1837 (2003).
[33] S. Ono and S. Kondo, *Encyclopedia of Physics* (Springer, Berlin, 1960), Vol. 10.
[34] A. B. Subramaniam, M. Abkarian, L. Mahadevan, and H. A. Stone, Nature (London) **438**, 930 (2005).
[35] W. C. Swope and H. C. Andersen, Phys. Rev. B **41**, 7042 (1990).
[36] M. E. Fisher, Physics (Long Island City, N.Y.) **3**, 255 (1967).
[37] M. Matsumoto, S. Saito, and I. Ohmine, Nature (London) **416**, 409 (2002).
[38] K. Binder, Z. Phys. B: Condens. Matter **43**, 119 (1981).
[39] A. V. Neimark and A. Vishnyakov, J. Chem. Phys. **122**, 174508 (2005).
[40] J. A. Barker and D. Henderson, Rev. Mod. Phys. **48**, 587 (1976).
[41] J. D. Weeks, D. Chandler, and H. C. Andersen, J. Chem. Phys. **54**, 5237 (1971).
[42] Y. Tang and B. C.-Y. Lu, AIChE J. **43**, 2215 (1997), see also Ref. 66.
[43] J. J. Nicolas, K. E. Gubbins, W. B. Street, and D. J. Tildesley, Mol. Phys. **37**, 1429 (1979).
[44] J. K. Johnson, J. A. Zollweg, and K. E. Gubbins, Mol. Phys. **78**, 591 (1993).
[45] T. Sun and A. S. Teja, J. Phys. Chem. **100**, 17365 (1996).
[46] L. G. MacDowell, J. Chem. Phys. **119**, 453 (2003).
[47] L. S. Schulman, J. Phys. A **13**, 237 (1980).
[48] K. Binder, Phys. Rev. A **25**, 1699 (1982).
[49] B. A. Berg and T. Neuhaus, Phys. Rev. Lett. **68**, 9 (1992).
[50] B. A. Berg, U. Hansmann, and T. Neuhaus, Z. Phys. B: Condens. Matter **90**, 229 (1993).
[51] N. B. Wilding, Phys. Rev. E **52**, 602 (1995).
[52] M. Müller and L. G. MacDowell, Macromolecules **33**, 3902 (2000).
[53] J. R. Errington, Phys. Rev. E **67**, 012102 (2003).
[54] P. Virnau and M. Müller, J. Chem. Phys. **120**, 10925 (2004).
[55] A. M. Ferrenberg and R. H. Swendsen, Phys. Rev. Lett. **61**, 2635 (1988).
[56] J. R. Errington, J. Chem. Phys. **118**, 9915 (2003).
[57] V. K. Shen and J. R. Errington, J. Chem. Phys. **122**, 064508 (2005).
[58] J. R. Errington and V. K. Shen, J. Chem. Phys. **123**, 164103 (2005).
[59] M. Müller and N. B. Wilding, Phys. Rev. E **57**, 2076 (1994).

[60] A. J. Yang, J. Chem. Phys. **82**, 2082 (1985).
[61] P. Virnau, M. Müller, and K. Binder (private communication).
[62] S. Punnathanam and D. S. Corti, Ind. Eng. Chem. Res. **41**, 1113 (2002).
[63] M. Mareschal, M. Baus, and R. Lovett, J. Chem. Phys. **106**, 645 (1997).

[64] H. E. Bardouni, M. Mareschal, R. Lovett, and M. Baus, J. Chem. Phys. **113**, 9804 (2000).
[65] M. E. Fisher and S.-Y. Zinn, J. Phys. A **31**, L629 (1998).
[66] Y. Tang and B. C.-Y. Lu, Fluid Phase Equilib. **190**, 149 (2001).